Journal of Power Sources 196 (2011) 2289–2297

Contents lists available at ScienceDirect

Journal of Power Sources

journal homepage: www.elsevier.com/locate/jpowsour

Simplified calculation of the area specific impedance for battery design

Kevin G. Gallagher*, Paul A. Nelson, Dennis W. Dees

Chemical Sciences and Engineering Division, Argonne National Laboratory, 9700 S. Cass Avenue, Lemont, IL 60439, USA

ARTICLE INFO

Article history:
Received 10 August 2010
Received in revised form 4 October 2010
Accepted 5 October 2010
Available online 13 October 2010

Keywords:
Battery design
Lithium ion
Area specific impedance
Charge transfer resistance

ABSTRACT

Battery design is a critical aspect of material and system development that leads to the commercialization of effective electrochemical energy storage systems. Successful modeling of battery designs relies upon accurate calculation of the area specific impedance (ASI). A simplified calculation of the ASI is presented that accounts for physical limitations without performing computationally expensive calculations. The limiting currents for transport within the electrolyte and within the intercalation materials are implemented into a linear form of the Butler–Volmer equation to calculate the interfacial impedance. Lithium-ion batteries are then designed to examine the effect of power to energy ratio on battery dimensions. A large ASI is shown to be detrimental to battery design regardless if the increase in impedance results from mass transport limitations or a reduction in electrochemical active area due to small electrode loadings. The smaller electrochemical active area does not increase the voltage losses of a battery when a constant C-rate is maintained. However, the higher ASI values from low electrode loadings require a larger separator and current collector area resulting in a greater battery volume and weight to achieve similar energy and power requirements when compared to a system with a lower ASI.

1. Introduction

The ability to calculate and project battery weight, volume, material requirements, and cost is extremely valuable to the research, industrial, and economic communities alike. This calculation is even more valuable if it is computed in an efficient and time effective manner while still producing meaningful and reasonably accurate results. To achieve this end, we have been developing relatively simple models that use experimentally measured electrochemical data, physical properties and proposed cell designs as inputs to the calculation. The model then allows the user to evaluate the battery design for various cell chemistries to meet various power and energy requirements.

The required experimental data is acquired through straightforward experiments. The reversible capacity and voltage profile of the positive and negative electrode materials at the cycling rate of interest (e.g. *C* or *C*/3) must be measured but is often available in the literature. Additionally, measurements of the area specific impedance (ASI) for the discharge rate used for energy and the rate used for power are required. In transportation applications, the battery must be able to achieve specified pulse discharge and charge conditions. The ASI for pulse power transportation applications can be measured using the hybrid pulse power characterization (HPPC) technique [1]. An example of the current and voltage behavior during a HPPC test may be found in Fig. 1. In the HPPC technique, the ASI is measured as a function of depth of discharge at 10% intervals. The current is pulsed in discharge mode for a period of time, presently 10 s. Then the current is stopped and voltage is allowed to relax. Next, the current is pulsed in the charge mode at typically 75% of the discharge value. The ASI is calculated separately for charge and discharge pulses, Eq. (1). *V* stands for the cell voltage and *I* represents the current density. The subscripts refer to value before the pulse, t0, and at the end of the pulse, t1.

$$\frac{V_{t0} - V_{t1}}{I_{t1} - I_{t0}} = \text{ASI} \tag{1}$$

The ASI is not an inherent constant of a specific battery chemistry or cell design. The measured value of the ASI is a complex combination of resistances within the battery resulting from the physical processes occurring at different length and time scales. Therefore, the measured value is a function of many factors (state of charge, pulse length, current density, C-rate, particle size, transport and kinetic parameters, etc). Three general approaches exist to account for the ASI in battery design modeling. First, one could systematically design and assemble a large number of cells with changing parameters and measure the resulting ASIs. Secondly, a complex physics based model could be used to predict the ASI for different electrode designs and then this could be used to predict a "scaled-up" battery design [2,3]. Finally, one could take the ASI to be constant over the range of designs studied. The last option is the simplest and thus is most commonly used in battery design models. Our previous battery design models assumed the ASI for

* Corresponding author. Tel.: +1 630 252 4473; fax: +1 630 252 4176.
E-mail address: kevin.gallagher@anl.gov (K.G. Gallagher).

0378-7753/$ – see front matter © 2010 Elsevier B.V. All rights reserved.
doi:10.1016/j.jpowsour.2010.10.020

Nomenclature

a	electrochemically active area per unit electrode volume, cm^{-1}
A	area, cm^2
ASI	area specific impedance, $\Omega\,cm^2$
c_j	concentration of lithium in region j, $mol\,cm^{-3}$
c_j^*	reference concentration of lithium in region j, $mol\,cm^{-3}$
C	cell capacity, Ah
D_{LiPF6}	diffusion coefficient of $LiPF_6$ based electrolyte, $cm^2\,s^{-1}$
D_s	diffusion coefficient of lithium in active material particle, $cm^2\,s^{-1}$
F	Faraday's constant, 96485.3 $C\,mol^{-1}$
i_0	exchange current per unit of interfacial area, $A\,cm^{-2}$
$\mathbf{i}_s$	superficial solution current in electrolyte phase, $A\,cm^{-2}$
i_n	transfer current per unit of interfacial area, $A\,cm^{-2}$
I	current density, $A\,cm^2$
I_{lim}^{ionic}	limiting current density for lithium ion transport through separator, $A\,cm^2$
I_{lim}^{ssDiff}	limiting current density for lithium diffusion in active material particles, $A\,cm^2$
L	region thickness, cm
N_{cell}	number of cells in the battery
P	battery power, W
r_C	C-rate, h^{-1}
r_p	diffusion length of active material, cm
R	universal gas constant, 8.3144 $J\,mol^{-1}\,K^{-1}$
t_{pulse}	duration of current pulse, s
t_+	transference of lithium ions with respect to the solvent
S	specific surface area, $m^2\,g^{-1}$
T	absolute temperature, K
Q	specific capacity, $Ah\,g^{-1}$
U	equilibrium potential, V
V	voltage, V
y	molar fraction of lithium in solid particles
z_+	charge of lithium ion
α_a	anodic transfer coefficient
α_c	cathodic transfer coefficient
δ	thickness, cm
ε	volume fraction
η	surface overpotential, V
κ	conductivity, $S\,cm^{-1}$
ρ	active material density, $g\,cm^{-3}$

Subscript and superscript

act	active material
batt	battery
const	constant
inact	inactive material
intf	interfacial
ocv	open circuit voltage
pos	positive electrode
neg	negative electrode
sep	separator
t0	before the pulse
t1	at the end of the pulse
void	void space of region filled with electrolyte
total	total contributions to cell sandwich ASI
+	lithium ions in the electrolyte
s	lithium in the active material particles
T	maximum lithium in the active material particles

a 1 cm^2 section of electrode to be constant for a specific chemistry and state of charge [4–8]. The ASI for the required duration of the pulse could then be accounted for by selecting the appropriate data point from the experimental measurement or using an equivalent circuit model to fit the experimental results. The selected value was then added to a calculated current collection system resistance based on a chosen cell design. While this approach is fast and reasonable under certain conditions, the assumption of a constant ASI for many disparate battery designs is physically unrealistic and may result in the prediction of batteries that are impossible to reproduce with experiments. The goal of this work is to present an improved approach to treating the ASI that maintains the speed and simplicity required while incorporating the necessary limitations resulting from the underlying electrochemical processes. We will use Li-ion chemistries as the basis for discussion throughout the remainder of the paper; although, the approach we will present is sufficiently general to be applied to a range of battery chemistries.

2. Model development

2.1. Formulation of ASI calculation

A schematic of a section of a Li-ion cell is depicted in Fig. 2. All three regions contain a void or porous phase that is filled with electrolyte. The separator region contains a polymer phase to prevent electron transport between the positive and negative electrodes while allowing electrolyte transport between these two regions. Each electrode is composed of solid particles of active material for intercalation and inactive materials that improves electronic conduction and/or structural integrity. The active materials are typically covered in a thin film formed from side reactions with the electrolyte referred to as the solid electrolyte interphase (SEI). The electrons move to/from the electrodes to their respective current collectors and in/out of the cell to the external circuit.

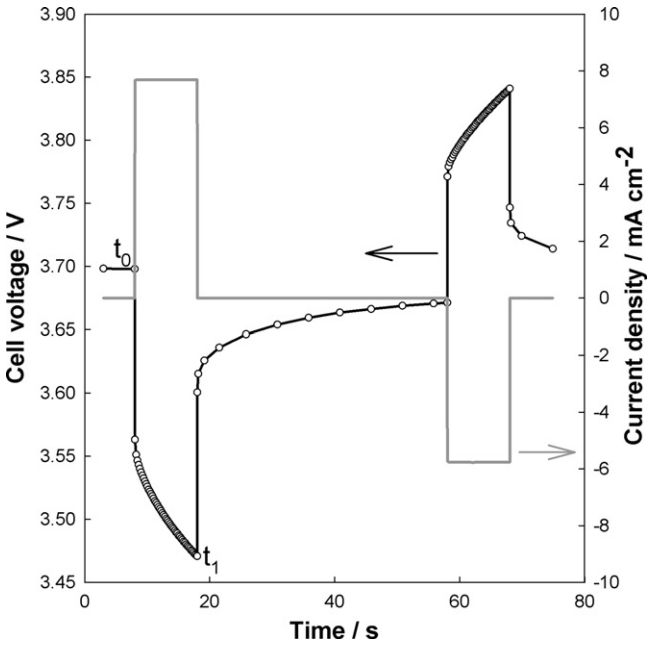

Fig. 1. Controlled current and observed voltage during a HPPC test.

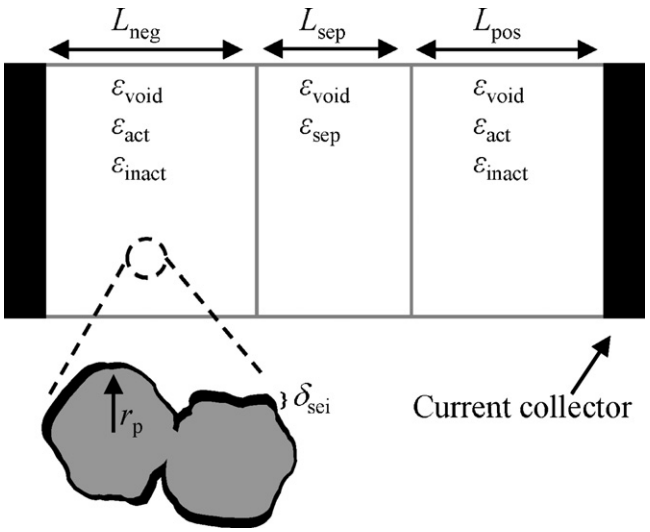

Fig. 2. An illustration of a segment of a full Li-ion cell. The volume fractions in each region sum to unity. All regions contain a void or porous phase that is filled with electrolyte.

The ASI is an experimentally measured value resulting from a collection of resistances that originate from transport and kinetic processes within the current collection components, electrolyte, active material, and their shared interfaces. The contribution to the ASI from the current collection system should be calculated separately to maintain simplicity and ease of use of the model. A large portion of the ohmic contribution to the ASI arises from ion transport through the electrolyte filled porosity of the electrode and separator, and any SEI that may be present on the active materials. An approximation of these resistances is found in Eq. (2) for the cell sandwich depicted in Fig. 2. This equation is only to serve as an introduction to some of the straightforward sources of impedance. The region thickness, L, void volume fraction, ε_{void}, electrochemically active area per unit volume, a, and thickness of the SEI, δ_{sei}, are most likely different for the positive and negative electrodes. The conductivity of the bulk electrolyte, κ_0, is significantly greater than the SEI, κ_{sei}. The ASI from ion transport within the pores of the electrode scales with one half of the electrode thickness assuming a constant current distribution throughout the depth of the electrode. Ohmic losses resulting from the transport of electrons through the electrode conducting matrix to the current collector must also be included in the ASI. The treatment of those will be discussed later in the paper.

$$\mathrm{ASI}_{\mathrm{Li}^+} \approx \left[\frac{L}{\kappa_0 \varepsilon_{\mathrm{void}}^{1.5}}\right]_{\mathrm{sep}} + \left[\frac{L}{2\kappa_0 \varepsilon_{\mathrm{void}}^{1.5}} + \frac{\delta_{\mathrm{sei}}}{\kappa_{\mathrm{sei}} aL}\right]_{\mathrm{pos}} + \left[\frac{L}{2\kappa_0 \varepsilon_{\mathrm{void}}^{1.5}} + \frac{\delta_{\mathrm{sei}}}{\kappa_{\mathrm{sei}} aL}\right]_{\mathrm{neg}} \quad (2)$$

The charge transfer resistance (CTR) component of the ASI is perhaps the most variant with changes in electrode design. We may examine the CTR by analyzing the Butler–Volmer equation often used to predict electrochemical reaction rates. The nonlinear dependence of current on potential can be simplified to a linear approximation for this discussion. An example of this linear formulation of electrochemical reaction rate per unit of interfacial area, i_n, is expressed in Eq. (3) [9].

$$i_n = i_0 \left(\frac{c_+}{c_+^*}\right)^{\alpha_a} \left(\frac{c_T - c_s}{c_T - c_s^*}\right)^{\alpha_a} \left(\frac{c_s}{c_s^*}\right)^{\alpha_c} \frac{(\alpha_a + \alpha_c)F}{RT}\eta \quad (3)$$

Here, i_0 is the exchange current density related to the interfacial area. R and T correspond to the universal gas constant and absolute temperature respectively. The subscripts on the concentration terms, c_j, are as follows: + is for the lithium ions in the electrolyte, s is for lithium in the solid active material and T is for the maximum lithium content in the solid. The surface overpotential, η, is the difference between the electrode potential, V, and the equilibrium potential, U. The transfer coefficients, α_a and α_c, are each taken to be 0.5 and thus sum to unity.

One must consider the relationship of the transfer current density, i_n, to the porous electrode of the electrochemical cell to analyze the CTR's role in the ASI. We consider the positive electrode for the first example. Porous electrode theory relates the divergence of the superficial electrolyte current of an electrode, i_s, to the rate of electrochemical reaction in Eq. (4) [10]. The reaction is treated as homogenous by the inclusion of a, the ratio of electrochemical surface area to electrode volume. The negative sign in Eq. (4) reflects the arbitrary decision to denote a discharge current as being positive valued. We choose the simplifying assumptions of a unidimensional, isothermal model while also neglecting gradients within the electrode to allow for lumped behavior. That is, we can consider the reaction to occur equally throughout the depth of the electrode, Eq. (5). This assumption is reasonable for small to moderate electrode thicknesses with slow interfacial kinetics or for a significant sloping open circuit potential versus state of charge curve that is common for the layered oxide intercalation compounds commonly used in Li-ion batteries.

$$\nabla \cdot \mathbf{i}_s = \frac{\partial \mathbf{i}_s}{\mathrm{d}x} = -a i_n \quad (4)$$

$$I = -a i_0 L_{pos} \left[\left(\frac{c_+}{c_+^*}\right)\left(\frac{c_T - c_s}{c_T - c_s^*}\right)\left(\frac{c_s}{c_s^*}\right)\right]^{0.5} \frac{F}{RT}\eta \quad (5)$$

The current density, I, is related to the geometric area of the electrode and chosen to be a positive value for discharge currents and negative value for charge currents. The concentration of the reactants is treated by accounting for the depletion of the species at higher current densities. Linear concentration profiles are assumed for Li^+ in the separator and within the solid particles. The limiting current, I_{lim}, for lithium transport is treated with a simplification of the concentration profile as a function of current, Eq. (6).

$$c_j = c_j^* \left(1 - \frac{I}{I_{lim}}\right) \quad (6)$$

This treatment will adequately provide for a dramatic increase in the CTR at the limiting current but not the more gradual increase due to moderate concentration polarization. Substitution of Eq. (6) into (5) results in Eq. (7).

$$I = -a i_0 L_{pos} \left\{\left(1 - \frac{I}{I_{lim}^{ionic}}\right)\left[1 - \left(\frac{I}{I_{lim}^{ssDiff}}\right)^2\right]\right\}^{0.5} \frac{F}{RT}\eta \quad (7)$$

The limiting current for ionic transport in the electrolyte and for solid state diffusion in the active material may be determined by separate calculations using diffusion coefficients and diffusion lengths. These values may also be verified with a detailed model based on concentrated solution theory and/or with experimental measurements. Our implementation for limiting currents represents a best case scenario and most likely overestimates the limiting currents for transport within the electrolyte and solid active material. The maximum flux of Li^+ through the solvent filled pores of the separator may be approximated using dilute solution theory and the Bruggeman correction for tortuosity [10]. Eq. (8) uses Faraday's law to convert the maximum flux into a current. Here, D_{LiPF6} is the diffusion coefficient of a commonly used electrolyte, z_+ is the charge of the cation, and t_+ is the cation transference number with respect to the solvent. The change in cation concentration is taken to be twice the initial concentration, $\Delta c_+ = 2c_{+,o}$. The role of electrolyte transport within the pores of the electrode is not treated in

this paper.

$$I_{\text{lim}}^{\text{ionic}} = \frac{z_+ F D_{\text{LiPF6}} \varepsilon_{\text{void}}^{1.5}}{1 - t_+} \frac{\Delta c_+}{L_{\text{sep}}} \tag{8}$$

The analogous limiting current for lithium diffusion within an intercalation particle is Eq. (9). The change in intercalated lithium concentration, $\Delta c_s = c_T(1-y)$, and solid state diffusion coefficient, D_s, both depend upon the normalized amount of lithium within the particle, y. If the particle is assumed to be at 50% state of charge (SOC), then $y = 0.5$. This equation is most likely a poor representation of the actual limiting current as the boundary conditions for the insertion particle are different than those of transport through the porous separator. The concentration profile within the particle is most likely nonlinear and thus an alternate approach to determining the limiting current is advisable. We choose to fit our limiting current to available published experimental data.

$$I_{\text{lim}}^{\text{ssDiff}} = a L_{\text{pos}} z_+ F D_s \frac{\Delta c_s}{r_p} \tag{9}$$

The electrochemical active area per unit volume may be related to the particle radius with the approximation $a = 3\varepsilon_{\text{act}}/r_p$. The benefit of reducing particle size is two-fold. The smaller particle size decreases the time constant for diffusion, $(r_p)^2/D_s$. Additionally, the electrochemical active area is inversely proportional to the particle radius. Thus, a smaller particle has significantly larger surface area for the electrochemical reaction to occur. The practical consequence of using smaller particles is that the electrode becomes less energy dense. The electrode void fraction is always higher for an electrode composed of small particles rather than large particles using current manufacturing techniques. A balance must be made between the rate capability of an electrode and the desired energy density.

The ASI for the positive electrode CTR is related to the kinetic expression by accounting for the change in the equilibrium potential as charge is passed, Eq. (10). The variables on the right hand side of the following equations pertain to the positive electrode unless otherwise stated. The superscript identifier is left off to improve the ease of reading. The concentration of lithium at the surface of the particle determines the equilibrium potential. One must know the dependence of the potential on the SOC and how the concentration of lithium in the particle will change during the pulse to calculate the thermodynamic contribution to the ASI. The equilibrium potential function for a positive electrode material is generally known and often reported in literature. We will use the slope of the known potential function and assume it is constant for small perturbations from a specified SOC. For example, a 10C pulse lasting 10 s is assumed to be a small perturbation as it removes less than 3% of the total lithium of an electrode. We note that it is common for potential functions to rapidly change near the end of discharge. This steep change will manifest as a large contribution to the ASI. The example we explore in later sections is based on materials at 50% SOC and thus the slope is not a strong function of concentration.

$$\text{ASI}_{\text{ctr}}^{\text{pos}} = \frac{V_{\text{t0}}^{\text{pos}} - V_{\text{t1}}^{\text{pos}}}{I} = \frac{U_{\text{t0}}^{\text{pos}} - V_{\text{t1}}^{\text{pos}}}{I} = -\frac{\eta}{I} - \frac{\Delta U}{I} = -\frac{\eta}{I} - \frac{\text{d}U}{\text{d}y}\frac{\text{d}y}{I} \tag{10}$$

The surface concentration of the particle is difficult to implement with the simplified approach used in this work. However, the change in the equilibrium potential with the average concentration, that which exists after a long relaxation period, is easily determined. To present the flux of lithium in the solid in a more intuitive way, the current density, I, is normalized to a C-rate, r_C, using Eq. (11). Here, the specific capacity, Q, the active material density, ρ, active material volume fraction, ε_{act}, and the electrode thickness, L, are used. The change in the average concentration of lithium that arises from the passage of current is shown Eq. (12) where t_{pulse} is the length of the current pulse. The final expression for the positive electrode ASI_{ctr} is represented by Eq. (13). Here, we account for the concentration polarization in the second term, η/I, while accounting for the thermodynamic factor with the third term, $\text{d}U/I$.

$$I = r_C Q \rho \varepsilon_{\text{act}} L_{\text{pos}} \tag{11}$$

$$\text{d}y \approx \Delta y = \frac{r_C t_{\text{pulse}}}{3600} \tag{12}$$

$$\text{ASI}_{\text{ctr}}^{\text{pos}} = \frac{RT}{a i_0 L_{\text{pos}} F}\left\{\left(1 - \frac{I}{I_{\text{lim}}^{\text{ionic}}}\right)\left[1 - \left(\frac{r_C}{r_{C,\text{lim}}}\right)^2\right]\right\}^{-0.5} - \frac{\text{d}U}{\text{d}y}\frac{t_{\text{pulse}}}{3600 Q \rho \varepsilon_{\text{act}} L_{\text{pos}}} \tag{13}$$

In practice, it is difficult to separate the CTR from the resistance of the transporting ions through the SEI. Both scale with $(aL)^{-1}$ and would require studies such as electrochemical impedance spectroscopy (EIS) to separate out the resistances based upon the relative time scales. Unfortunately, EIS does not unequivocally provide an answer to this question since the analysis of the spectrum relies upon assumptions of which processes are occurring. We choose to sum the two resistances together in an effort to accurately capture the observed behavior. The interfacial ASI for the positive electrode may then be considered in Eq. (14).

$$\text{ASI}_{\text{intf}}^{\text{pos}} = \frac{1}{L_{\text{pos}}}\left[\frac{\delta_{\text{sei}}}{a\kappa_{\text{sei}}} + \frac{RT}{a i_0 F}\left\{\left(1 - \frac{I}{I_{\text{lim}}^{\text{ionic}}}\right)\left[1 - \left(\frac{r_C}{r_{C,\text{lim}}}\right)^2\right]\right\}^{-0.5} - \frac{\text{d}U}{\text{d}y}\frac{t_{\text{pulse}}}{3600 Q \rho \varepsilon_{\text{act}}}\right] \tag{14}$$

The remaining contributions to the ASI must be accounted for to compare Eq. (14) with experimental ASI measurements. We choose to lump the remaining resistances into a parameter, $\text{ASI}_{\text{const}}$, which will vary only with differing SOC. Therefore, all changes to the ASI with electrode thickness, current density, or C-rate will result from the interfacial impedance in Eq. (15).

$$\text{ASI}_{\text{total}} = \text{ASI}_{\text{intf}}^{\text{pos}} + \text{ASI}_{\text{intf}}^{\text{neg}} + \text{ASI}_{\text{const}} \tag{15}$$

2.2. Determination of the parameters

The parameters used in Eq. (15) are a combination of measured, fitted, and calculated values. The determination of interfacial parameters such as resistivity of the SEI or exchange currents is challenging. Not surprisingly, the reported values for exchange currents and SEI parameters vary widely throughout the literature. Consequently, we choose to assume one of the sources of the resistance is dominate. The impedance of the positive electrode SEI is usually small, especially at the beginning of life. Therefore, we neglect the SEI contribution to the positive electrode interfacial ASI for the following calculations in this paper. The equilibrium potential function for the positive electrode is taken from the work of Dees et al. [11] with 50% SOC is defined at a open circuit cell voltage of 3.68 V. The slope of the potential function is approximately −1 at this SOC. The positive electrode exchange current will be fit to experimental ASI measurements and thus include the contribution from the SEI. We adopt a value of 50 $\Omega\,\text{cm}^2$ for the negative electrode interfacial ASI based upon the single particle measurements of Dokko et al. [12–14]. This impedance is based on particle surface area calculated with the radius. Therefore, we

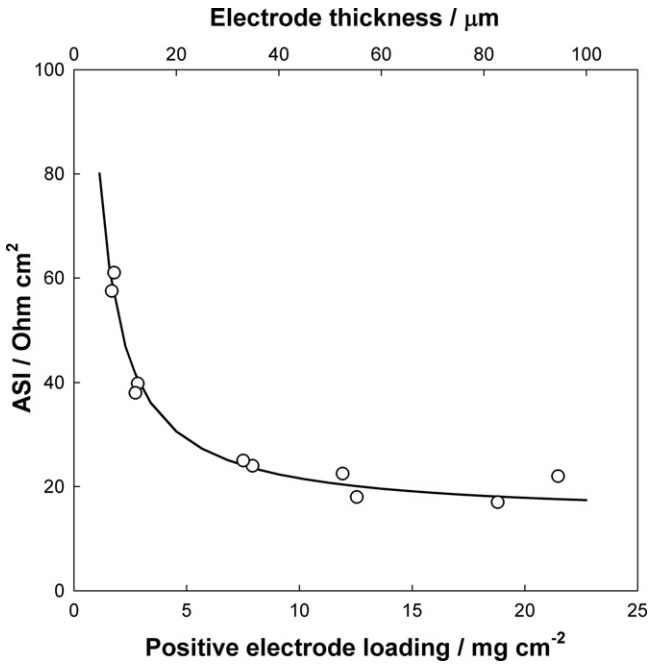

Fig. 3. Experimentally measured ASI values (open circles) from [15] compared to fit (solid line) from Eq. (15).

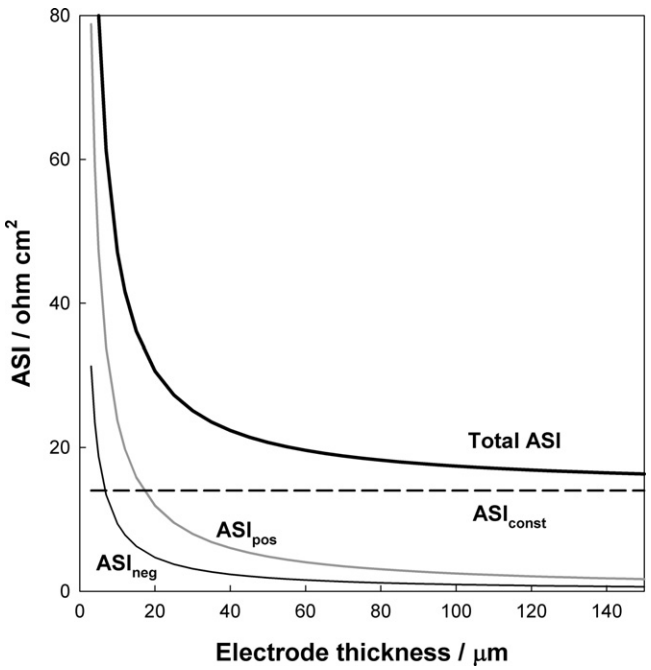

Fig. 4. The total ASI is composed of contributions from the positive and negative interfacial impedance and the lumped constant parameter. The positive electrode interfacial impedance dominates the total ASI at low electrode thicknesses.

use the particle radius for our chosen graphite to estimate the electrochemical active area. We ignore limiting currents in the negative electrode based upon the focus on discharge behavior and high performance communicated by Dokko et al. [13]. The diffusion coefficients for the electrolyte are taken from Dees et al. [11] with $D_{LiPF6} = 1.1 \times 10^{-6}$ cm^2 s^{-1} for the electrolyte used in the experimental measurements. We use the experimental data for current pulses from Abraham et al. to define the limiting C-rate as 27 h^{-1} [16].

Fig. 3 compares the fit of Eq. (15) to experimentally measured ASI values for 2032-type coin cell configurations with varying positive electrode thicknesses from the work of Lu et al. [15]. The ASI shown is for 10 s 1.8*C* discharge pulses from a coin cell at 50% SOC. The parameters used for the fit are shown in Table 1. All cells are based on a positive electrode active material of $LiNi_{0.80}Co_{0.10}Al_{0.05}O_2$ (NCA) layered oxide (Fuji CA1505) and a negative electrode based on G8 graphite from Conoco Philips. The manufacturer reports an average particle size of 8 μm and a specific surface area of 2 m^2 g^{-1} using the BET method. The thickness of the graphite is varied to maintain an excess negative electrode capacity of 1.1–1.5 compared to the positive electrode. The separator is Celgard 2325 and the electrolyte is 1.2 M $LiPF_6$ in EC:EMC (3:7 by weight).

Good agreement is achieved between the model and the full cell data with only two fitting parameters, i_0 and ASI_{const}. The ASI is nearly constant for electrode thicknesses greater than 40 μm. In contrast, the positive electrode dominates the ASI at small electrode thicknesses for the full cell measurements, Fig. 4. The change in positive electrode equilibrium potential is responsible for approximately one third of the positive electrode interfacial impedance. The contribution of the negative electrode interfacial impedance is never more than 25% of the positive. The lumped parameter most likely captures some of the complicated interfacial behavior from both electrodes.

Abraham et al. used a reference electrode cell to study the ASI as a function of pulse magnitude for a NCA/Mag-10 graphite cell [16]. Fig. 5 compares the measured and calculated ASIs for 18 s discharge pulses from a full-cell balanced to a 35 μm thick positive electrode at 50% SOC. The limiting C-rate was fit to the experimental data

Table 1
Parameters used in Eq. (15) to fit experimental data.

Property	Symbol	Graphite	NCA	Units
Specific reversible capacity	Q	310	150	mAh g^{-1}
Exchange current	i_0	N/A	0.63	mA cm^{-2}
Particle radius	r_p	4	5	μm
Electrochemical active area	a	4667	2893	cm^{-1}
Active material density	ρ	2.25	4.74	g cm^{-3}
Active volume fraction	ε_{act}	0.62	0.48	
Void volume fraction	ε_{void}	0.32	0.32	

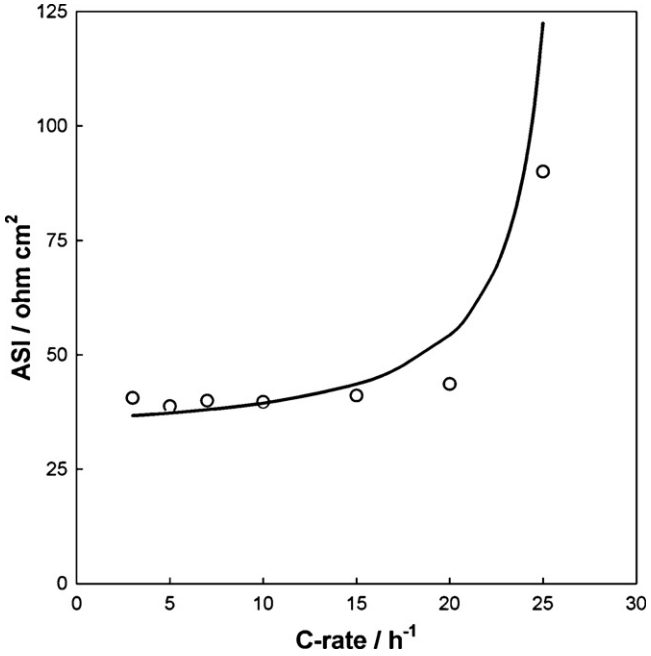

Fig. 5. Comparison of the ASI for 18 s discharge pulses from [16] (open circles) to the model (solid line). The limiting current was fit to the values seen here.

shown and is only significant close to the limiting value of 27 h^{-1}. The lumped parameter, ASI_{const}, was increased to match the larger ohmic losses in the reference electrode cell of the Abraham et al. The larger ohmic losses are the result of electrical contact resistances between the electrode foil and current collector and the double separator surrounding the reference electrode. The good fit is verification that the approach taken in this model is sufficient to provide reasonably accurate results to feed into a battery design model.

2.3. Limitations of the model

A more rigorous approach would treat the competing effects that occur within the porous electrode. The current distribution in the porous electrode is rarely ever totally uniform. In most current Li-ion cells, the solid matrix conductivity is much higher than the electrolyte conductivity. The ease of electron transport in the solid phase (i.e. near constant potential) has the effect of shifting the current density towards the separator–electrode interface to minimize the ohmic losses in the electrolyte. The set of equations used to accurately predict the current potential behavior has been widely accepted; however, many parameters require determination and computation is not trivial [9,10,17,18]. Euler and Nonnenmacher and then Newman and Tobias treated this complex problem with simplifications [10,19,20]. An analytical solution has been presented that allows the current distribution to vary along the electrode thickness as dictated by the current density, reaction kinetics, and ohmic losses. To achieve this end, the concentration of the reactant is assumed constant and film resistances are not treated. We have compared this analytical solution with our more empirical approach. Our proposed ASI calculation achieves a better fit with the experimental data than the analytical solution of Euler and Nonnenmacher especially in the transition from a constant ASI to the steep increase at small electrode thicknesses. This agreement may be fortuitous, but the failure of the early analytical porous electrode solution most likely results from the complex mass transport occurring within the pores of the electrode, intercalation particles, and the film that serves as the interphase.

The limitations of the proposed approach are a result of the simplifications used to enable quick calculations. The equation is derived for the linear regime of the Butler–Volmer equation. This typically applies for low to moderate C-rates in the Li-ion battery system. The exponential dependence of the full Butler–Volmer equation is likely to be important for higher C-rates. Furthermore, this approach assumes an isothermal cell design. This assumption may be reasonable if the designed deviation from open circuit voltage is a low value. For example, we typically design batteries that achieve maximum power at only 80% of the open circuit voltage. Inclusion of the full Butler–Volmer equation and the heat generation will lower measured ASI values. However, we also do not account for uneven current distributions in the porous electrode structure that will increase measured ASIs. In addition, the ionic limiting current is approximated for a steady state condition. Higher currents are most likely possible for short durations as the concentration of the reactants will be higher in the initial moments the current is passed. The level of accuracy achieved with our stated assumptions is reasonable to achieve the goal of the model. The intention of this work is to provide a realistic result that can guide the battery designer's intuition or feed into other models.

3. Results and discussion

3.1. The dependence of the ASI on electrode thickness and C-rate

The effect of electrode thickness and C-rate on the ASI may be evaluated using Eq. (15) for the NCA–graphite full cell. Fig. 6 displays the change in calculated ASI as the C-rate is varied from 5*C* to 20*C*. The two different limiting currents affect the ASI in distinct ways. The ASI quickly increases to an infinite value as the current density reaches the ionic limiting current (i.e. at large electrode thicknesses). The maximum achievable electrode thickness decreases with increasing C-rate. This is because the current density passing through the separator increases with increasing electrode thickness (capacity), at constant C-rate, until it approaches the limiting current. In contrast, the ASI at all electrode thicknesses increases as the C-rate approaches the solid state diffusion limited current. In this analysis, one can see the interplay between C-rate and current density. In actual Li-ion cells, the increase in impedance will begin at much lower current densities and C-rates as the concentration gradients build in the cell. The goal of our calculation is to set a physical limitation to the cells one might design, not to precisely capture the current–voltage behavior.

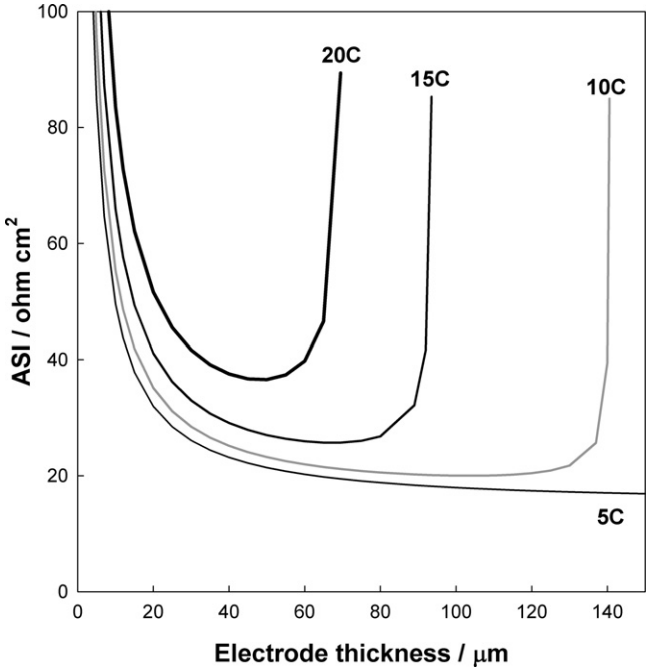

Fig. 6. The effect of limiting currents on the ASI may be examined by changing the C-rate as a function of electrode thickness.

An interesting feature of the ASI at constant C-rate is the increase in impedance as the electrode thickness decreases. Dees et al. previously simulated the same NCA–graphite system with a robust model based on porous electrode and concentrated solution theories [11]. Their results also predict the steep increase in ASI with decreasing electrode thickness. The work presented here explains the consequences of this increased ASI in the context of the end battery design. This behavior is a direct result of the inverse relationship of the ASI to electrode thickness contained in Eq. (14). At constant C-rate, the current density decreases as the electrode thickness decreases and thus the rise in ASI is cancelled out by the diminishing current. This is best demonstrated by examining the voltage loss incurred from the positive electrode CTR. Multiplication of Eq. (13) by (12) results in Eq. (16) with $f(I)$ representing the limiting current expression. Inspection of Eq. (16) reveals the voltage loss from the interfacial impedance does not depend on the electrode thickness if the C-rate is held constant. Clearly, voltage losses will increase if the current density is held constant as electrode thickness is reduced.

$$\Delta V = r_C Q \rho \varepsilon_{act} \frac{RT}{a i_0 F} f(I) - \frac{dU}{dy} \frac{r_C t_{pulse}}{3600} \quad (16)$$

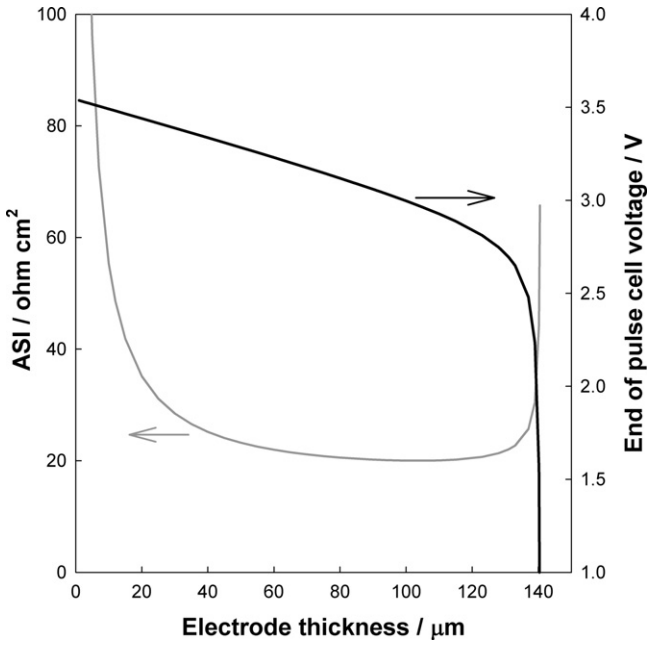

Fig. 7. The effect of the ASI on cell voltage at the end of a 10 s 10*C* discharge pulse for a NCA–graphite full cell.

Fig. 7 displays the cell voltage at the end of a 10*C* pulse that is 10 s in duration as a function of positive electrode thickness. This is the V_{t1} value used in Eq. (1). The cell voltage was determined by using the open circuit voltage, $V_{t0} = U_{t0} = 3.68$ V, for a NCA–graphite full cell at 50% SOC. The ASI is also shown for the same conditions. The steep rise in the ASI at low electrode thickness does not result in increased polarization of the cell unlike at large thicknesses. On the other hand, the limiting current provides for a severe drop in cell voltage at the maximum electrode thickness for this C-rate.

3.2. Implementation in battery design model

The role of changes in the ASI on battery design may be evaluated using the Argonne Battery Design model which has been communicated previously [4–8]. The fitted ASI equation from above is implemented into an iterative scheme that calculates current collection resistance, material quantities, and battery size for a specified power and energy. The present cell design is based on a prismatic pouch cell configuration with a thickness of 10 mm and a length to width aspect ratio of 1.3. The positive and negative electrode tabs are drawn out of opposite ends and are nearly as wide as the cell to minimize ohmic losses. The current collection components depend on the size of the cells but typically add only $\sim 0.5\,\Omega\,\mathrm{cm}^2$ to increase the $\mathrm{ASI}_{\mathrm{total}}$ to the $\mathrm{ASI}_{\mathrm{batt}}$ for the batteries designed below (calculation not shown for brevity). The area of the positive electrode, Eq. (17), is found from $\mathrm{ASI}_{\mathrm{batt}}$, battery power, P, voltages, V, and number of cells, N_{cell}. The difference between the open circuit voltage, V_{ocv}, and the cell voltage, V_{cell}, is the polarization of the cell. The negative electrode is taken to be 1 mm longer than the positive electrode in both length and width to alleviate concerns of lithium plating during charge pulses. The separator area is slightly larger than the negative electrode to prevent the electrical shorting.

$$A_{\mathrm{pos}} = \frac{\mathrm{ASI}_{\mathrm{batt}} P}{N_{\mathrm{cell}} V_{\mathrm{cell}} (V_{\mathrm{ocv}} - V_{\mathrm{cell}})} \tag{17}$$

The positive electrode thickness, Eq. (18), is determined from the capacity of the cell, C, specific capacity of the electrode, and the positive electrode area. The negative electrode thickness is determined by the specific capacity of the negative electrode and the designed excess capacity to prevent lithium plating during charging. We have chosen a ratio of 1.25 negative to positive capacity for this study.

$$L_{\mathrm{pos}} = \frac{C}{Q \rho \varepsilon_{\mathrm{act}} A_{\mathrm{pos}}} \tag{18}$$

We have calculated a number of high P/E ratio batteries to highlight the role of changes in the interfacial ASI on battery design. All batteries have a specified power of 25 kW reached at 80% of the open circuit voltage using one insulated module containing 20 cells connected in series. We define the power of a battery based upon the pulse power characteristics at a specific SOC. Batteries used in a hybrid electric vehicle require a high power to energy (P/E) design and typically operate at 50% SOC. The usable energy of these cells is assumed to be 25% of the total energy measured at a *C*/3 discharge rate. The capacity of each cell changes to meet the stated energy requirement. Our battery design model explicitly accounts for the physical dimensions and weights of all components such as cell materials, current collection, module casing, and thermal insulation, for example. The results for a NCA–graphite system are displayed in Fig. 8.

The FreedomCAR energy storage goals target P/E ratios of 16–20 for power-assist hybrids batteries [1]. For the battery chemistry studied here, a local minimum in battery weight and volume is found near a P/E ratio of $17\,\mathrm{h}^{-1}$ (1.8 kWh). The maximum power density (i.e. minimum weight and volume) is located at the knee in the ASI curve. The battery design model reduces the electrode thickness as the required energy is lowered. The decreasing electrode thickness causes the ASI to increase as the CTR of the positive electrode becomes significant as discussed earlier. Fig. 9 illustrates the dramatic increase in cell area as the energy requirement and thus electrode thickness are reduced. This relation is a direct result of the interdependence of the ASI, L, and A_{cell} as discussed earlier.

Fig. 10 clearly shows the C-rate is the only significant source of polarization from the two limiting current mechanisms considered. The C-rate increases as the P/E ratio increases at lower designed battery energies. The current density remains less than one half of

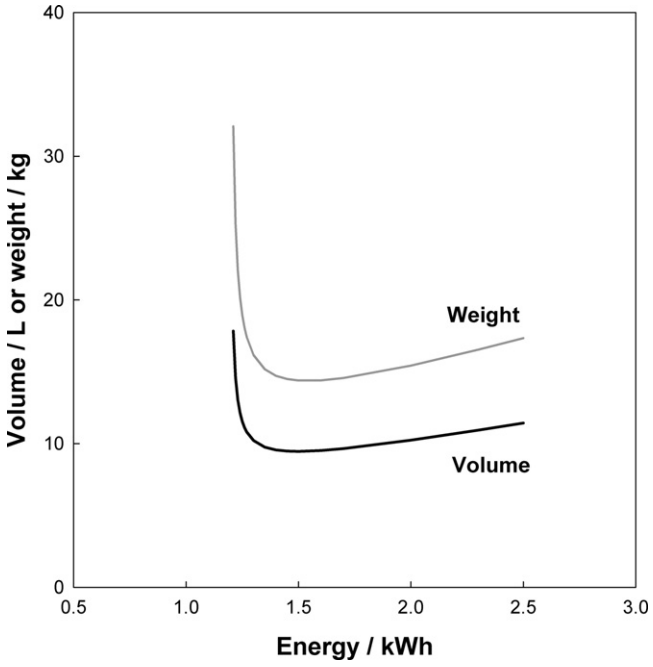

Fig. 8. Effects of battery pack energy on battery volume and weight for 20-cell, NCA–graphite packs delivering 25 kW power surges for 10 s at 80% of OCV.

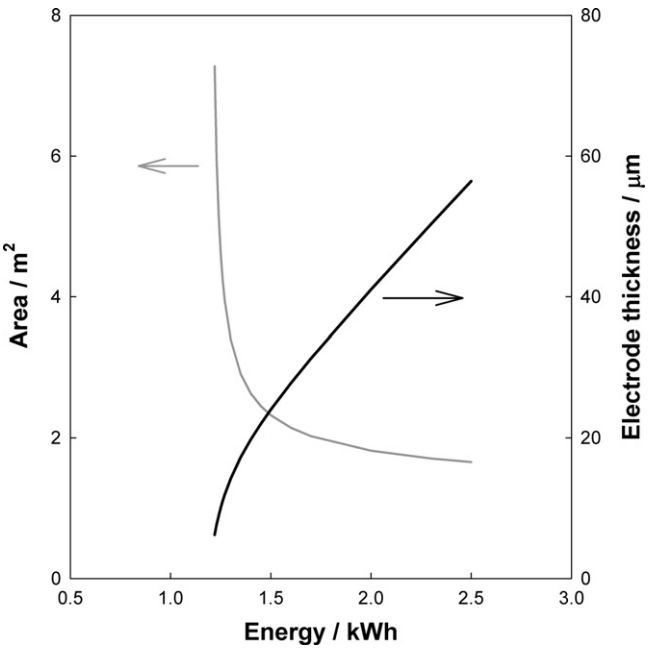

Fig. 9. Effects of battery pack energy on positive electrode area and thickness.

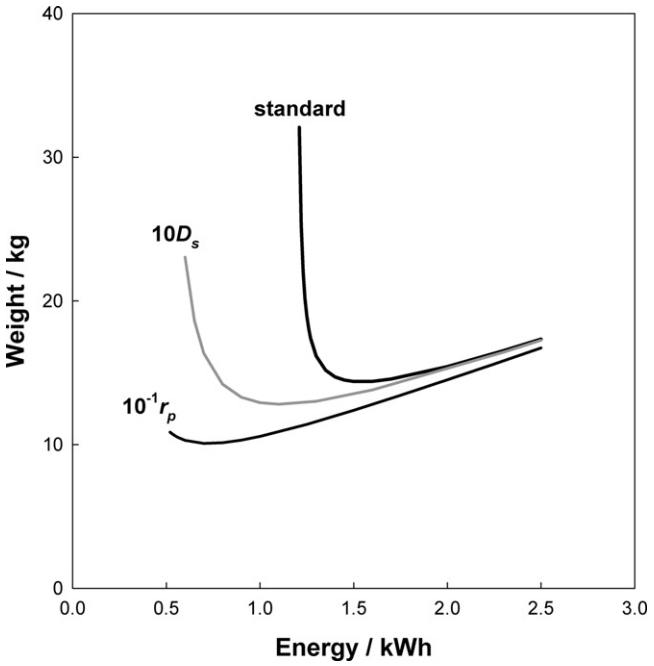

Fig. 11. The effect from increasing the solid state diffusion coefficient ($10D_s$) and separately reducing particle size ($10^{-1}r_p$) is shown on the battery design. Reducing particle size increases the limiting C-rate and reduces the charge transfer resistance.

the limiting value and is dramatically reduced as the area of the cell is increased (e.g. ASI increases). In fact, the total current is the same for all battery designs here as a result of specifying that maximum power will be achieved at a set fraction of the open circuit voltage. Therefore, doubling the number of cells in a battery from 20 to 40 reduces the capacity of the cell by half through a reduction in cell area. The calculated electrode thickness and current densities remain the same as they are governed by the fraction of the open circuit voltage at which the maximum power is achieved.

The effect of the positive electrode CTR on battery design may be examined by changing various parameters such as the solid state diffusion coefficient and the particle size. Fig. 11 shows the change in battery weight and volume with $10D_s$ and $10^{-1}r_p$. These choices reflect possible material changes that could be used to meet battery power and energy density requirements. The reduction in particle size has the strongest effect on battery design by lowering the impedance and thus weight for all P/E designs considered. The change in void volume or porosity of the electrode with particle size has not been included. This could be easily implemented with an empirical correlation, but the change in void fraction from 33% to 50% has only a minor effect on battery size compared to the decrease in ASI. Reducing particle size may result in other detrimental effects. The increase in specific surface area of the particle will increase side reactions with the electrolyte. This will amplify the rate of power and capacity fade while possibly exacerbating safety issues. Therefore, blending of electrode materials has been implemented to include materials that have high power density with those that have high energy density [21].

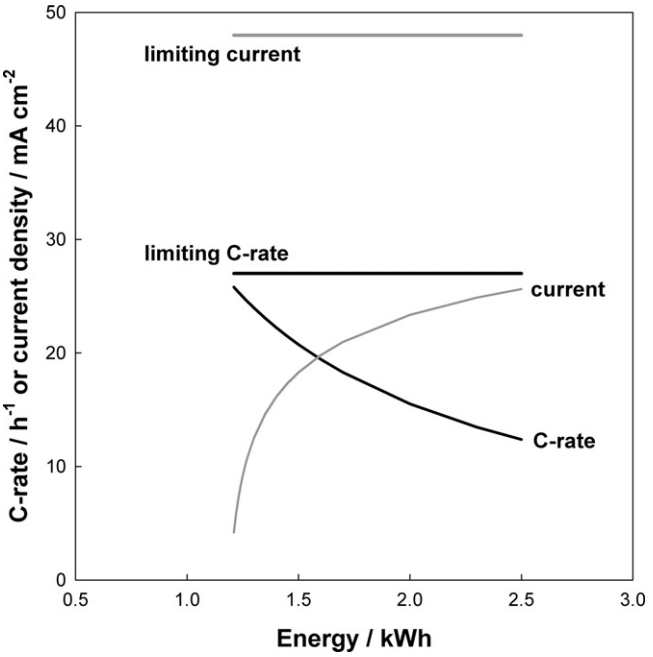

Fig. 10. Current density (thin grey line) and C-rate (thin black line) as a function of battery energy for the 25 kW design. The limiting current density (thick grey line) and limiting C-rate (thick black line) are also shown for comparison.

The operating conditions of a battery system should be chosen with sufficient room for changes to the limiting currents. As electrochemical systems age, the porosity of the separator may decrease and some fraction of the intercalation materials may become inactive. These two symptoms of aging will lower the limiting current of the system. The performance of the battery will be severely hindered if the designed operating current reaches a value close to the limiting currents. The design of an electrochemical system should always consider the lifetime capability of the system rather than only initial performance.

4. Conclusions

A simplified expression for the ASI has been presented and implemented into a battery design model. The accuracy of predictions made by the model has been greatly improved by implementing physical limitations in the interfacial impedance expression. This iterative approach is very efficient and allows for rapid study of a number of different scenarios. Furthermore, a battery design model with this simplicity may easily feed information into other models such as economic plant design models

or other simulations that use many repetitive calculations [22,23]. The combination of accuracy and ease of calculation help to connect laboratory studies to commercial product development.

Acknowledgements

Financial support from the U.S. Department of Energy is gratefully acknowledged. The submitted manuscript has been created by UChicago Argonne, LLC, Operator of Argonne National Laboratory ("Argonne"). Argonne, a U.S. Department of Energy Office of Science Laboratory, is operated under Contract No. DE-AC02-06CH11357. The U.S. Government retains for itself, and others acting on its behalf, a paid-up, nonexclusive, irrevocable worldwide license in said article to reproduce, prepare derivative works, distribute copies to the public, and perform publicly and display publicly, by or on behalf of the Government.

References

[1] INEEL, FreedomCAR Battery Test Manual for Power-Assist Hybrid Electric Vehicles, 2003.
[2] P. Albertus, J. Couts, V. Srinivasan, J. Newman, Journal of Power Sources 183 (2) (2008) 771–782.
[3] C. Fellner, J. Newman, Journal of Power Sources 85 (2) (2000) 229–236.
[4] P. Nelson, K. Amine, A. Rousseau, H. Yomoto, International Electric Vehicles Symposium, EVS-23, 2007.
[5] P. Nelson, I. Bloom, K. Amine, G. Henriksen, Journal of Power Sources 110 (2) (2002) 437–444.
[6] P. Nelson, D. Dees, K. Amine, G. Henriksen, Journal of Power Sources 110 (2) (2002) 349–356.
[7] P.A. Nelson, G.L. Henriksen, K. Amine, Power Sources for the New Millennium, Proceedings 2000 (22) (2001) 245–256.
[8] R.F. Nelson, Journal of Power Sources 91 (1) (2000) 2–26.
[9] K.E. Thomas-Alyea, R.M. Darling, J. Newman, in: W. van Schalkwijk, B. Scrosati (Eds.), Advances in Lithium-Ion Batteries, Kluwer Academic Publishers, New York, 2002, 345 pp.
[10] J. Newman, K.E. Thomas-Alyea, Electrochemical Systems, 3rd ed., John Wiley & Sons, Inc., Hoboken, NJ, 2004.
[11] D. Dees, E. Gunen, D. Abraham, A. Jansen, J. Prakash, Journal of the Electrochemical Society 155 (8) (2008) A603–A613.
[12] K. Dokko, Y. Fujita, M. Mohamedi, M. Umeda, I. Uchida, J.R. Selman, Electrochimica Acta 47 (6) (2001) 933–938.
[13] K. Dokko, N. Nakata, Y. Suzuki, K. Kanamura, Journal of Physical Chemistry C 114 (18) (2010) 8646–8650.
[14] M. Umeda, K. Dokko, Y. Fujita, M. Mohamedi, I. Uchida, J.R. Selman, Electrochimica Acta 47 (6) (2001) 885–890.
[15] W. Lu, A. Jansen, D. Dees, P. Nelson, N. Veselka, G. Henriksen, Journal of Power Sources 196 (2010) 1537–1540.
[16] D.P. Abraham, D.W. Dees, J. Christophersen, C. Ho, A.N. Jansen, International Journal of Energy Research 34 (2) (2010) 190–203.
[17] T.F. Fuller, M. Doyle, J. Newman, Journal of the Electrochemical Society 141 (4) (1994) 982–990.
[18] T.F. Fuller, M. Doyle, J. Newman, Journal of the Electrochemical Society 141 (1) (1994) 1–10.
[19] J. Euler, W. Nonnenmacher, Electrochimica Acta 2 (1960) 268–286.
[20] J.S. Newman, C.W. Tobias, Journal of the Electrochemical Society 109 (12) (1962) 1183–1191.
[21] J.W. Fergus, Journal of Power Sources 195 (4) (2010) 939–954.
[22] P. Nelson, Plug-in 2009, Long Beach, CA, 2009.
[23] P.A. Nelson, D.J. Santini, J. Barnes, International Electric Vehicles Symposium EVS-24, Stavanger, Norway, 2009.